Materials and Design 182 (2019) 108044

Contents lists available at ScienceDirect

Materials and Design

journal homepage: www.elsevier.com/locate/matdes

Materials with enhanced adhesive properties based on acrylonitrile-butadiene-styrene (ABS)/thermoplastic polyurethane (TPU) blends for fused filament fabrication (FFF)

A.S. de León *, A. Domínguez-Calvo, S.I. Molina

Dpto. Ciencia de los Materiales, I. M. y Q. I., IMEYMAT, Facultad de Ciencias, Universidad de Cádiz, Campus Río San Pedro, s/n, 11510 Puerto Real, Cádiz, Spain

HIGHLIGHTS

- Design of novel materials for fused filament fabrication with enhanced adhesive properties.
- Correlation of properties at macro and micro/nanoscale.
- Study of the compatibility of thermoplastic and thermoplastic elastomers by spectroscopic and microscopic analysis.
- ABS-based material that allows 3D-printing without heating the platform.

GRAPHICAL ABSTRACT

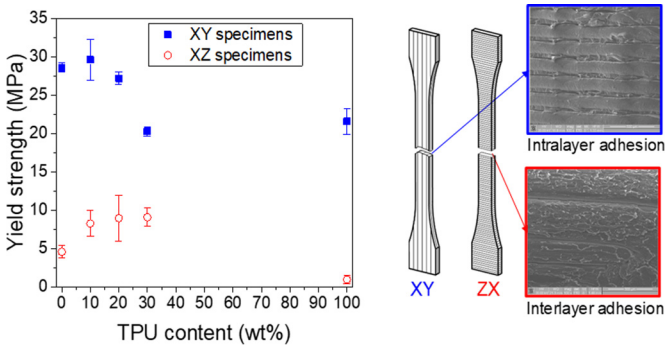

ARTICLE INFO

Article history:
Received 13 June 2019
Received in revised form 13 July 2019
Accepted 15 July 2019
Available online 16 July 2019

Keywords:
Additive manufacturing
3D printing
Fused filament fabrication
Fused deposition modeling
Polymer blends
Adhesion
Interlayer bonding
Mechanical properties
Material characterization

ABSTRACT

In the current work, we prepared a novel material suitable for additive manufacturing by using acrylonitrile-butadiene-styrene (ABS) copolymer as matrix and a thermoplastic polyurethane (TPU) as additive. Conditions for successful printing via fused filament fabrication (FFF) were optimized for the ABS:TPU blends. Compatibility of ABS and TPU in the blends was studied by Fourier-transformed infrared (FTIR) spectroscopy, showing the appearance of new supramolecular interactions via hydrogen bonding. Compositional studies were carried out by confocal Raman microscopy and atomic force microscopy (AFM), demonstrating the good compatibility between the two compounds. Mechanical and adhesive properties were studied by 3D-printing different normalized test specimens in different directions. It was shown that blends containing 10–20 wt% TPU led to enhanced adhesion between layers without loss in yield strength, while 30 wt% TPU led to a good adhesion between layers and to the printing platform when printing at room temperature.

1. Introduction

Additive manufacturing (AM) has increased in the last years due to its versatility and flexible production of highly customizable products. Contrary to traditional (subtractive) manufacturing, AM techniques

* Corresponding author.
E-mail address: alberto.sanzdeleon@uca.es (A.S. de León).

https://doi.org/10.1016/j.matdes.2019.108044

fabricate objects using a layer-by-layer approach from a digital model [1]. Potential benefits include complex design of internal features, lightweight manufacturing with hollow or lattice structures, competitive cost production, drastic reduction of waste and easy scalability [2].

One of the most widespread AM techniques is fused filament fabrication (FFF, also called fused deposition modeling, FDM) presents a number of advantages like widespread use, easy usability and reduced cost compared to other AM techniques. Fabrication via FFF implies optimizing parameters like printing temperature and speed, platform temperature, raster orientation, infill density, layer height or flow. All these parameters have an influence on the final mechanical properties of the fabricated object and the optimal values strongly depend on the material used [3]. Feedstock materials for FFF are usually plastics. In particular, one of the most widespread is acrylonitrile-butadiene-styrene (ABS) copolymer due to its good mechanical properties at a competitive cost [4]. In order to obtain materials with enhanced mechanical or functional properties, many groups have developed ABS-based printable composites with fillers such as graphite [5], metals [6], lignin [7], carbon fiber [8] or other polymers [9] as additives.

However, there are still a number of challenges to overcome to print objects via FFF with similar properties than objects fabricated using traditional techniques [10]. Mechanical properties can decrease down to 50% when FFF specimens are compared to samples fabricated with the same material by injection molding [11,12]. In particular, it has been reported that ABS tensile yield strength decreases from 49.94 to 27.59 MPa [13]. Lack of homogeneous distribution of the material and the presence of intrinsic porosity due to air gaps between the layers and roads of the deposited material causes this decrease in mechanical properties. This makes the printed objects more brittle and with high anisotropy. This anisotropy can be easily quantified because yield tensile strength decreases significantly in the build-up direction when compared with any of the other two directions [14].

Different strategies have been followed to overcome these problems. Finite element analysis has been made to map the forces distribution when different external loads are applied to be able to predict the fractures modes and locations [15]. Other authors have performed studies of bond strength stablishing differences between physical and chemical bonds to understand the mechanisms happening during failure [16]. In general, influence of different parameters such as raster angle, printing direction on fracture toughness has been widely investigated and it has been proven that orientation of the object is highly important regardless of the material used [17–19].

However, lack of consensus about how to properly measure experimentally the adhesion between layers makes difficult to perform robust and comparable studies. For instance, Turk et al. [20] reported different mechanical properties of ABS, polyamide and polyamide composite with fibers for normalized specimens. They correlated yield strength measured for vertically printed specimens with adhesion between layers. Other groups have modified the feedstock material to reduce the anisotropy. For instance, Levenhagen et al. achieved to reduce the anisotropy by using bimodal molecular weight PLA or adding star-shaped molecules as additives [21,22]. Like previous authors, they printed standardized specimens in different directions to evaluate their mechanical properties. Complementarily, they also measured interlayer fracture resistance, using a previously developed T-peeling method [23]. Zhu et al. [24] also studied the interfacial bonding adhesion by varying the content of styrene-acrylonitrile (SAN) in an ABS matrix. For this study, they used rectangular, non-standard specimens. Davis et al. [25] proposed an alternative method to measure the mechanical strength not only between layers but also between two consecutive roads within a same layer. They defined these adhesive interactions as "weld strength". Riddick et al. [26] has also investigated the influence of build direction and raster orientating in ABS but testing standardized specimens. They observed that raster orientations of $\pm 45°$ led to higher softening material due to shear response. They also evidenced the anisotropy by showing the differences in tensile strength ranging from 12.42 MPa for vertically printed tensile specimens to 34.17 MPa for horizontally printed specimens with raster orientations of 0° (axial direction). Anisotropy has not only been observed in mechanical properties but also for thermal conductivity, evidencing its importance in the design of functional materials [27].

Other of the limitations of the FFF technology is the necessity of heating the printing platform to achieve a correct adhesion of the first layer. Otherwise, cooling speed of the deposited material is too fast and causes material detachment due to warping caused by thermal contraction [28]. Depending on the material used, minimum temperature needed is rather different. For instance, polylactic acid (PLA) can be printed without heating the platform temperature, while it needs to be heated to at least 90 °C for a correct printing of ABS [29].

To solve these problems, thermoplastic elastomers (TPE) are potential candidates as additives due to their good adhesive properties. Different types of TPE based on different polymers (vulcanized rubber, TPV; styrene, TPS; or polyurethane, TPU) have been reported to be printable without need of heating the platform temperature. TPE have high elongation at break ($\varepsilon_B > 100\%$) but low yield strength when compared to engineering polymers such as ABS [30]. Previous report on ABS:TPS printed blends showed that overall mechanical properties of the material decreased but no adhesion between layers was investigated [31]. On the other hand, Yin et al. [32] showed enhanced interfacial bound strength between ABS and TPU polymers due to good intermolecular diffusion. However, in this study polymers were not blended but printed separately.

In the current research, we present a series of ABS:TPU blends with TPU contents ranging from 10 to 30 wt%. We demonstrate that these blends can be successfully printed by FFF. We show that due to new intermolecular interactions and good compatibility of TPU and ABS, adhesive properties between layers and onto the building platform are enhanced while good overall mechanical properties are still maintained.

2. Materials and methods

2.1. Materials

ABS and TPU were purchased from Smart materials (Spain). Mechanical properties provided by the supplier are shown in Table 1. Materials were dried for at least 2 h at 80 °C prior to extrusion.

2.2. Extrusion of filament

Filament was prepared in a single-screw extruder (Noztek, UK) at a temperature of 230 °C with a screw speed of 60 rpm. At least 50 g of filaments of 1.75 ± 0.10 mm diameter were extruded. Blends were composed of 10 wt%, 20 wt% and 30 wt% TPU and 90 wt%, 80 wt% and 70 wt% ABS respectively.

2.3. Testing FFF samples

A Creality CR10 3D printer with a nozzle diameter of 0.4 mm was used to print damples with a surface of 1 cm^2 consisting of monolayers (0.02 cm height) for compositional studies (Fig. 1a)), 1BA test specimens according to ISO 527-2 (Fig. 1b)) and samples consisting of monolayers to evaluate material adhesion to the platform ($2.0 \times 12 \times 0.02$ cm, Fig. 1c)). 1BA test specimens were printed in two different directions, labelled as XY and XZ according to ISO/ASTM 52921:2013 (Fig. 1d)).

Table 1
Mechanical properties included in the technical data sheet issued by the fabricant.

	ABS	TPU
Young's modulus (MPa)	2030	12
Yield strength (MPa)	29.3	20.0
Elongation at break (%)	2.4	660

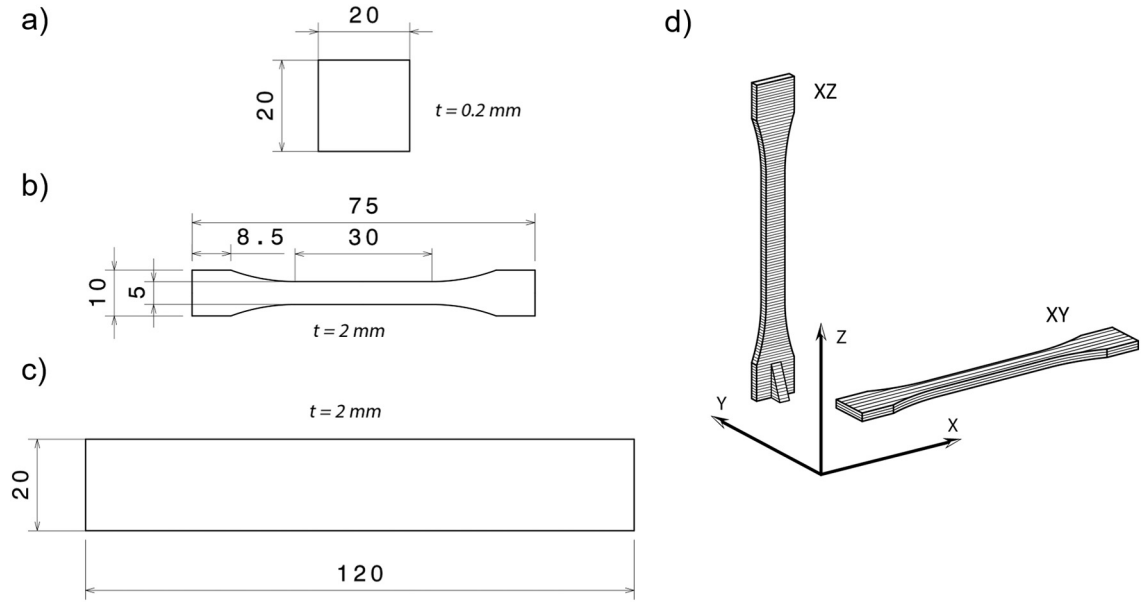

Fig. 1. Designs of a) Monolayers for compositional studies; b) 1BA tensile test specimens and c) monolayers to study influence of platform temperature on first layer adhesion; d) different orientations of the tensile test specimens.

At least 5 samples of each type were printed using pure ABS, pure TPU and blends containing 10, 20 and 30 wt% TPU. Digital files were created using Ultimaker Cura v 3.3.1 software. Nozzle temperature was set to 230 °C for all specimens. Printing speed was 30 mm/s for all samples, except for vertically printed test specimens, where printing speed was decreased down to 8 mm/s. Objects were printed following a lineal pattern with a raster angle of 0° (X axis and infill density of 100% in all cases. Wall speed, top speed and bottom speed were set as half of the printing speed in all cases. Travel speed was set to 120 mm/s. Retraction speed were set to 60 mm/s and 7 mm. Flow rate was 100% and layer height was 0.2 mm in all cases. Platform temperature was set to 90 °C regardless of the material printed for 1BA test specimens. When printing monolayers, platform temperature was ranged from room temperature (25 °C) to 90 °C, to study the influence of TPU content in platform adhesion. No supports were generated for none of the objects printed. The rest of the parameters were left as default by the software.

2.4. Material characterization

Surface roughness was measured using a Marh 2S Perthometer scanning instrument. Lengths ranging from 2.6 to 6 mm were measured at 3 different random positions along the planes XY and XZ in at least 3 different samples. For every measurement, average roughness (Ra) and mean width of the profile (RSm) were obtained and results were averaged. Fourier transform infrared (FTIR) spectroscopy analysis was carried out using a Bruker IFS 66 FT-IR spectrophotometer in attenuated total reflectance mode (ATR) in the range of 4000–650 cm^{-1} with a spectral resolution of 4 cm^{-1}. At least 3 spectra were taken for 3 independent printed samples were to ensure reproducibility of results. Raman microscope (alpha300, WITec) was used. The microscope was equipped with a piezo scanner (P-500, Physik Instrumente) and a 50× objective (Nikon, NA 0.6). A linearly polarized laser ($\lambda = 785$ nm) was focused onto the sample with a polarization angle of 0° and no analyzer in the light path. The Raman scattered light was detected on a thermoelectrically cooled CCD detector (DU401A-BV, Andor) with an integration time of 2 s. Single spectra were taken in at least 5 different regions of the sample. Atomic Force Microscopy (AFM) was performed in a Veeco Multimode Nanoscope IIIA (Bruker) operated in tapping mode under ambient conditions. Images were taken in regions of 5 μm × 5 μm. Tensile testing of specimens was performed in a Universal testing machine (Shimadzu) at a constant speed of 1 mm/min according to ISO 527-2. At least 5 specimens were tested and Young's modulus, yield strength and elongation at break values were dissected for each one of the specimens measured. Young's modulus was calculated as the slope between 0.05% and 0.25% strain on a stress-strain plot. Yield strength was obtained as the stress value where an increase in strain does not result in an increase in stress (maximum value in the Y axis). Elongation at break was obtained as the strain value in the rupture point (maximum value in the X axis). Results were averaged and standard deviations were presented as error bars. Analysis of variance (ANOVA) with a significance level of $\alpha = 0.05$ and Turkey test were performed to determine whether there were any statistically significant differences between the results. Fracture surface analysis was performed using a scanning electron microscope (SEM) FEI-Quanta 200 3D (Thermo Fisher). Samples were coated with a layer of Au in a Balzers SCD 004 Sputter Coater prior to scanning.

3. Results and discussion

3.1. Fabrication of filaments and samples for FFF printing

A single-screw extruder, previously heated at 230 °C, was fed with a mixture of ABS and TPU pellets containing either 10, 20 or 30 wt% TPU. Filament produced was reprocessed in the same extruder to ensure a good homogeneous distribution of TPU in the ABS matrix and a continuous filament of 1.75 ± 0.10 mm was obtained.

Then, printing conditions were carefully optimized before fabricating any sample. Our goal was to find a set of parameters valid for ABS, TPU and all ABS:TPU blends so all the different printed samples after could be directly comparable. Although ABS and TPU have been widely used in FFF, their optimal printing conditions are significantly different. Low printing temperature may cause insufficient flow because the filament is not fully molten while if it is too high it decreases the viscosity of the melt and can cause a poorly printed object or even degrade the material. Fabricant recommends to print ABS at 230–250 °C, while TPU can be printed from 200 °C. In our case, we checked that 250 °C was a too high temperature for TPU and led to its degradation (extruded filament was blackened) and printing below 230 °C led to poor quality samples for pure ABS. Thus, we decided to set printing temperature to 230 °C, which led to printable objects for all materials used, including ABS:TPU blends. In terms of printing speed, ABS can be printed at values of 50 mm/s without decreasing mechanical properties [33], but at these

values TPU filament is clogged within the gears of the printer, so speed was decreased down to 30 mm/s, which led to successfully printed samples. For vertically printed test specimens, printing speed was slowed down to 8 mm/s to ensure a correct printing, since this specimen is quite unstable even with the design shown in Fig. 1. Platform temperature was set to 90 °C, since otherwise ABS would detach from the platform after extrusion due to thermal contraction and TPU can be printed at any platform temperature. No adhesive spray or external agents were used, to avoid altering the composition or adhesion of the blends studied, since this may interfere with further characterization experiments, especially in the case of samples consisting of printed monolayers. Once these printing parameters were optimized (see the Materials and methods section), all samples were successfully printed. Roughness surface analysis was performed to evaluate the quality of the objects printed. Fig. 2a) shows the values of average roughness (Ra) of surfaces in the XY and XZ planes of the printed objects. These values were averaged from at least 3 different measurements of 3 different samples. Ra values of the objects in the XY plane are very much alike and in the range of the values reported in literature for pure ABS [34], so in principle it is expected that objects printed with ABS:TPU blends possess similar surface quality than pure ABS. In XZ plane, contrary to what expected, Ra increased with TPU content. This might occur because we are printing in some conditions that are valid for all our blends, but are not necessarily the optimal for pure TPU. Mean width of the profile (RSm) values (Fig. 2b) in this plane show that, except for pure ABS roughness values are around 200 μm with a very high precision (coefficient of variation <2% for all the blends). RSm can be associated with the height of layer in FFF, which matches quite well with the theoretical value. This indicates that, at least for the chosen printing conditions, the presence of TPU in the blends enhances the build-up process. ABS printed objects show a RSM of ca. 160 μm, which seems to evidence that ABS presents a higher contraction when cooling after filament deposition. After evaluating these results, we consider that objects can be successfully printed without major defects and acceptable surface finishing.

3.2. Material characterization

Squared monolayers of 1 cm^2 size were used to perform compositional characterization via FTIR. Fig. 3a) shows the spectra for ABS, ABS:TPU blends containing 10, 20 and 30 wt% TPU and TPU. FTIR spectra of the blends were normalized to the ABS 2237 cm^{-1} C≡N stretching peak for comparative purposes. As expected, blends contain the characteristic peaks for both pure ABS and TPU. FTIR has also been used for long time for detecting supramolecular interactions, in particular hydrogen bonding, by observing displacements in the peaks of the bonds involved [35]. In our case, we paid attention to C═O stretching and N—H bending, which are characteristic bonds present in TPU molecules regardless of the synthesis method. It is well-known that TPU can form intermolecular hydrogen bonding bridges. However, these interactions can be disrupted in presence of other compounds. For pure TPU, Fig. 3a) shows two peaks in the C═O stretching area, at 1730 and 1705 cm^{-1}. These peaks correspond to free and hydrogen bonded carbonyl, respectively [36,37]. Although these peaks are still visible in ABS:TPU blends, the peak at 1705 cm^{-1} is not sharped anymore and it looks more like a shoulder. For clearer interpretation, intensity ratios between hydrogen bonded and free C═O peaks were estimated. For pure TPU, this ratio is of 0.62, while for the three ABS:TPU blends ranged between 0.33 and 0.43. This clearly indicates that in presence of ABS, C═O groups present in TPU participate in hydrogen bonding interactions to a fewer extent. In the N—H bending region, we can observe a clear peak at 1531 cm^{-1} for pure TPU. This sharped peak is displaced and broadens towards higher wavenumbers for all the ABS:TPU blends studied. This evidences that presence of ABS is able to break intermolecular hydrogen bonds between C═O and N—H groups of TPU and interact forming new hydrogen bonds with the N—H [38]. These bonds are more likely to be formed by polar groups, as the C≡N group present in ABS. For instance, Chen et al. [39] evidenced the interactions between TPU and polar groups of PLA and graphene oxide. Moreover, there are also several reports that evidence the interaction between N—H groups and π interactions of aromatic rings [35,40]. Thus, we believe the styrene rings present in ABS can also interact with TPU. Fig. 3b) depicts the expected different supramolecular interactions in ABS:TPU blends.

Complementarily to FTIR analysis, Raman microscopy was performed in these samples. Single spectrum of ABS, TPU and the different ABS:TPU blends were taken in at least 5 different spots and results were averaged. As for FTIR, spectra obtained from ABS:TPU blends were normalized to the C≡N stretching peak for direct comparison. Fig. 4a) shows characteristic peaks for ABS at 1012 cm^{-1} corresponding to the ring breathing mode of polystyrene and at 2237 cm^{-1} corresponding to the C≡N bond stretching and characteristic peaks for TPU at 1731 cm^{-1} corresponds to C═O stretching and 1531 cm^{-1} corresponding to the amide II peak [41,42]. Fig. 4a) shows simultaneously peaks for ABS and TPU in all the blends studied. It can be observed that TPU characteristic peaks increase proportionally with the TPU content in the blends. This is a first indication of good compatibility between ABS and TPU in the blends, since we cannot identify separated regions of ABS and TPU, at least within the spatial resolution of the Raman laser. To investigate more in detail the chemical composition of the ABS:TPU blends, XY Raman mappings of the blends were performed [43]. To do

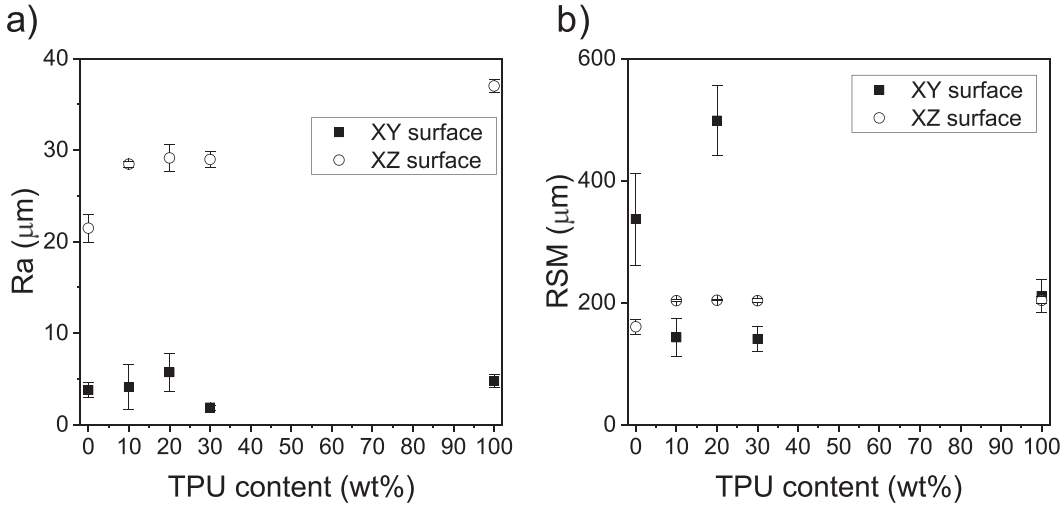

Fig. 2. a) Mean roughness (Ra) and b) root mean square roughness (RSM) values of surfaces in the X axis (filled squares) and Z axis (hollow circles).

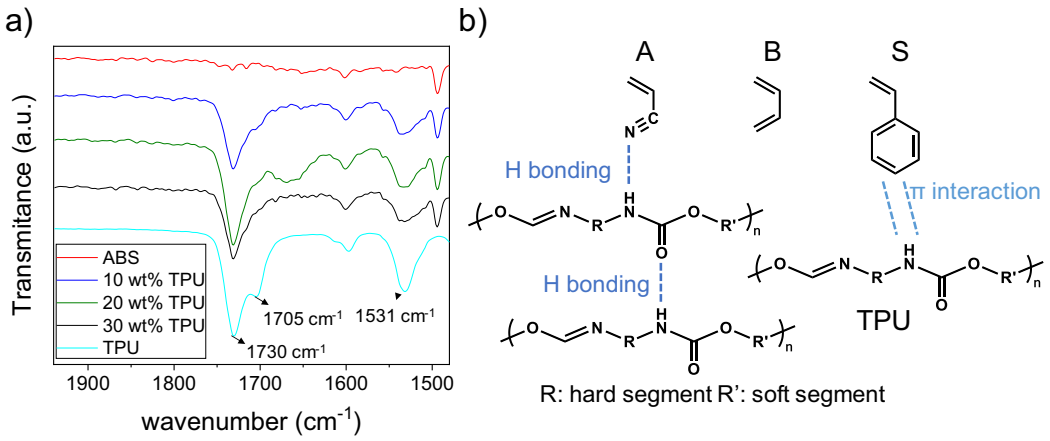

Fig. 3. a) Average FTIR spectra of pure ABS (red), ABS:TPU blends containing 10 wt% TPU (blue), 20 wt% TPU (green), 30 wt% TPU (black) and pure TPU (light blue); b) molecular structure of monomers present in ABS, TPU and expected supramolecular interactions. (For interpretation of the references to color in this figure legend, the reader is referred to the web version of this article.)

so, a region of 70 × 70 μm^2 was analyzed and characteristic signal at 1012 cm^{-1} was assigned to ABS while 1531 cm^{-1} was assigned to TPU. Fig. 4b)–c) show Raman mappings of ABS and TPU for a sample prepared with 20 wt% TPU. Darker areas correspond to lower intensity of the characteristic peaks studied, caused by possible roughness of the sample but most likely by sample degradation due to strong laser

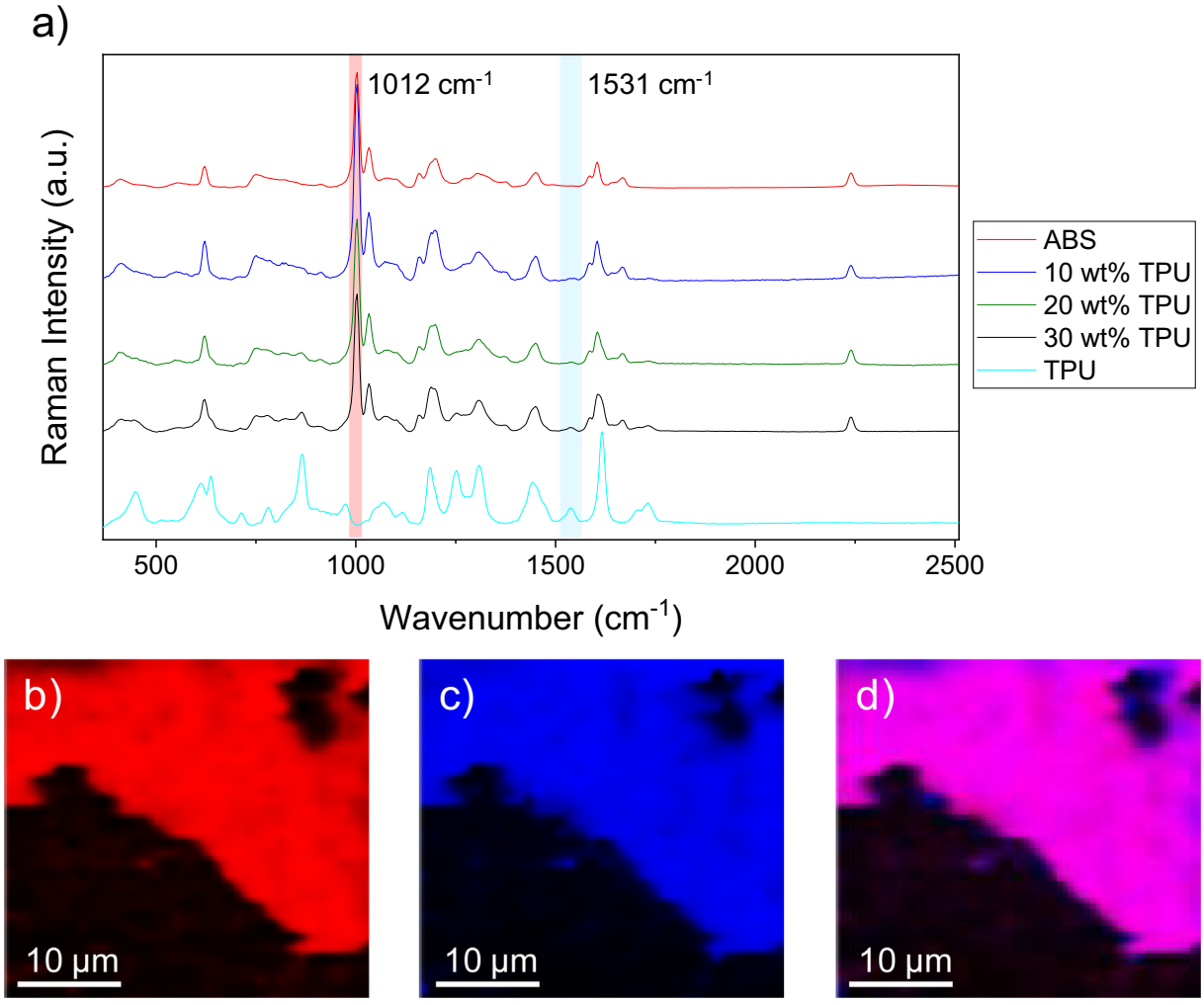

Fig. 4. a) Average Raman spectra of pure ABS (red), ABS:TPU blends containing 10 wt% TPU (blue), 20 wt% TPU (green), 30 wt% TPU (black) and pure TPU (light blue); b–c) Raman micrographs of blends containing 20 wt% TPU. Red area indicates the ABS characteristic peak at 1012 cm^{-1} while blue area corresponds to characteristic peak of TPU at 1531 cm^{-1}. These peaks were taken to perform Raman microscopy images shown for b) ABS, c) TPU and d) merged signals from ABS and TPU. (For interpretation of the references to color in this figure legend, the reader is referred to the web version of this article.)

radiation. Even though laser power was reduced so signal could be acquired but sample damage was minimal, it can be observed that Raman signal decreases in the lower part of the image. In the areas where these intensities are high enough to acquire enough signal, it can be observed that it varies in the same manner both for ABS and TPU. When merged (Fig. 4d)), no areas with higher signal of either of both components is observed, indicating a homogeneous distribution of both compounds. Due to the numerical apparatus of the microscope objective (50×) and wavelength of the laser (λ = 785 nm), lateral resolution of these spectra was calculated to be ~1 μm, so we state that there is no phase segregation in ABS and TPU blends, at least at microscale. This result shows that ABS and TPU present good compatibility, which is not trivial, since ABS and TPU present quite different chemical structure (see Fig. 3b)). For instance, it has been previously reported phase segregation for different polymeric blends including elastomeric thermoplastics and polyethylene [44]; thermoplastics and rubber [45] or thermoplastics, resins and clays [46]. Raman results are also in good agreement with FTIR analysis, which showed that there have been formed new supramolecular interactions between ABS and TPU, which probably helps to increase the compatibility with each other.

In an attempt to identify distribution of ABS and TPU in the blends, AFM experiments were performed. In particular, phase channel of AFM tapping mode was used to detect the different compounds in polymeric blends since it gives qualitative information about the hardness of the surface with nanometric resolution. It can be found in literature various examples related to copolymers [47], polymer composites [48] or, as it is our case, industrial polymer blends [49].

Fig. 5 shows comparative 25 μm^2 size images for ABS, blends containing 10, 20, and 30 wt% TPU and TPU. Height images in Fig. 5a)–e) show that surface topography is quite rough. It is important to consider that for samples fabricated via FFF the material is deposited with a controlled size of ca. 400 μm (nozzle diameter) and goes through conformational changes caused by the coefficient of thermal expansion during cooling process, which can lead to uncontrolled topology. Thus, we consider that height changes observed (<500 nm) in the regions analyzed are acceptable considering printing process conditions.

In the same areas, information from the phase channel was also analyzed. All phase mappings were normalized to the same values (0–60°) so all the images could be directly comparable. Fig. 5f) shows the phase mapping of pure ABS, where in this conditions a quite homogeneous light brown can be identified. In a similar fashion, Fig. 5j) shows the phase mapping of pure TPU, where a homogeneous dark brown, is shown. Taking these two images as reference, we can then identify the different polymeric phases in the surfaces printed with 10 wt% TPU (Fig. 5g)), 20 wt% TPU (Fig. 5h)) and 30 wt% TPU (Fig. 5i)). In these figures we can observe different contrasts of well-defined light brown and dark brown, that could be directly associated with colors shown in Fig. 5f) and j) for ABS and TPU, respectively. Areas of the darker phases were analyzed for Fig. 5g)–i) and values of ca. 9%, 16% and 29% were obtained. These values follow the trend of the theoretical content of TPU in the blends, and seem to confirm that dark brown color observed corresponds to TPU. It also supports the fact that we are observing the different phases with a submicrometric resolution, as we expected from the Raman results shown in Fig. 4d). In Fig. 5g), we can observe the TPU is organized forming lamella-like domain with a high aspect ratio within the ABS matrix. This can be correlated to the extrusion procedure during FFF, that leads to preferential roads and can be considered for future applications where FFF can be used for the formation of nanopatternings with polymer blends. These preferential directions in TPU regions decrease gradually when TPU content is increased to 20 and 30 wt%. In these cases, TPU domains tend to be larger and not necessarily homogeneously distributed within the ABS matrix. It can be observed in some cases that these domains are even interconnected, especially for blends containing 30 wt% TPU, where there are areas of ABS embedded in TPU domains.

3.3. Mechanical and adhesive properties

Test specimens of ABS, TPU and ABS:TPU blends containing 10, 20 and 30 wt% TPU were printed according to ISO 527-2 in two different directions (see Fig. 1d in the Materials and methods section for more details). This was done in order to evaluate the material mechanical properties (XY specimens), as well as the adhesive forces between layers during the printing process (XZ specimens) [33].

Fig. 6a)–b) shows representative strain-stress curves for ABS, TPU and blends containing 10, 20 and 30 wt% TPU for XY and XZ specimens. As expected, a high difference in the mechanical behavior can be observed depending on the orientation of the specimens printed. Interface between two contiguous layers has been shown to be the weakest region in FFF printed materials, due to inefficient diffusion of the material (i.e. polymeric chains) which leads to a high anisotropy of the material [50]. For clearer comparison, characteristic parameters of these curves (Young's modulus, yield strength and elongation at break) have been dissected from at least 5 samples, averaged and compared in Fig. 6b)–d). It can be observed that Young's modulus and yield strength of XY specimens follow a general trend, decreasing gradually when TPU

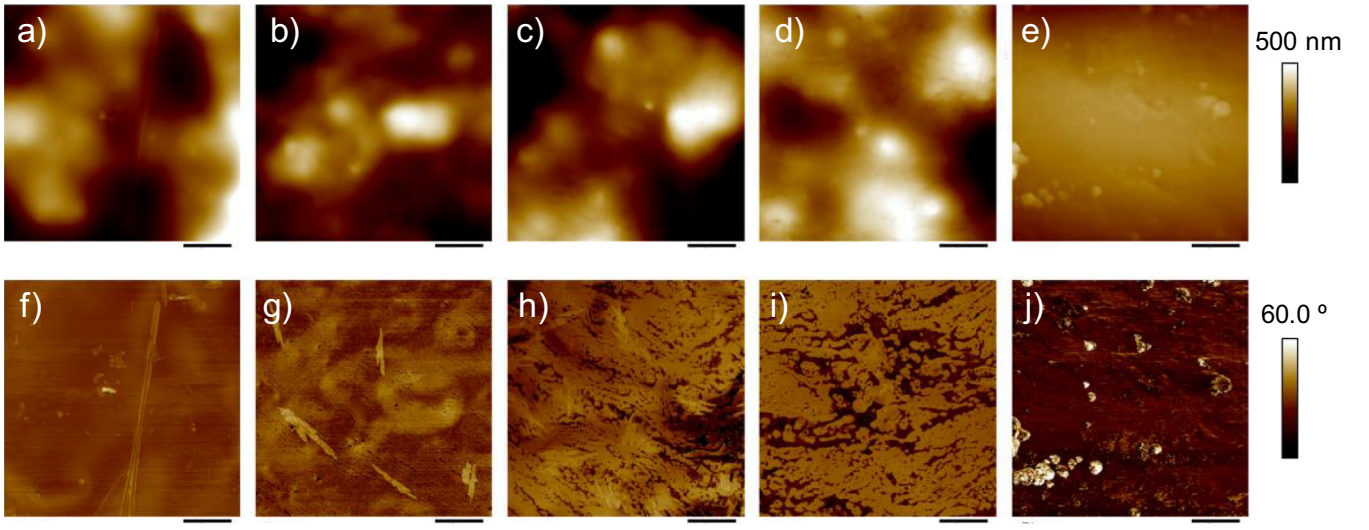

Fig. 5. AFM height images of a) pure ABS, ABS:TPU blends containing b) 10 wt% TPU, c) 20 wt% TPU, d) 30 wt% TPU and e) TPU; AFM phase images of f) pure ABS, ABS:TPU blends containing g) 10 wt% TPU, h) 20 wt% TPU, i) 30 wt% TPU and j) pure TPU. All images have been normalized to the same values to allow direct comparison. Scale bar: 1 μm.

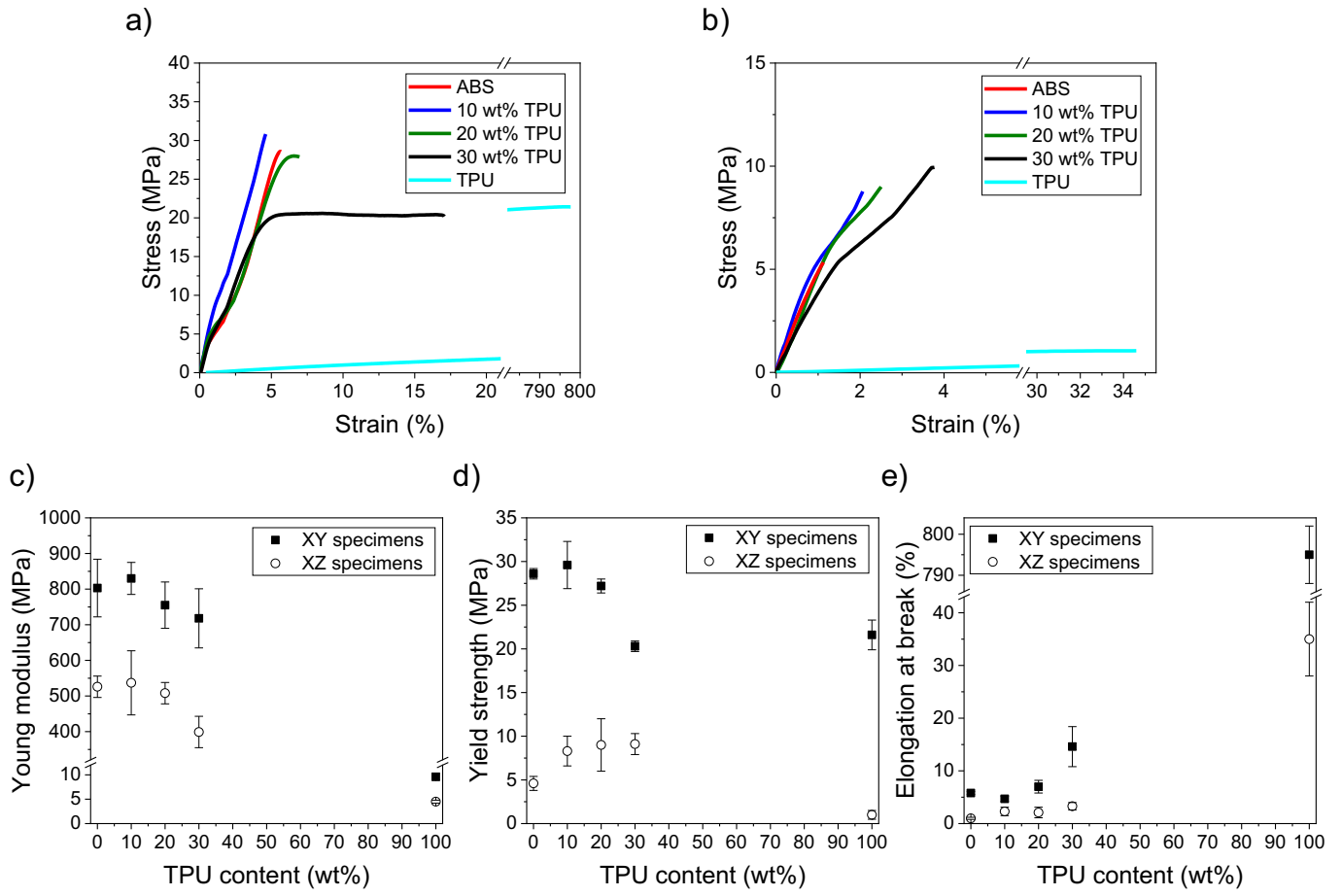

Fig. 6. Strain-stress representative curves of a) XY and b) XZ tensile testing specimens; c) Young's modulus, d) yield strength and e) elongation at break as a function of TPU content for XY and XZ specimens.

content is increased. Young's modulus values are comparable to those of pure ABS (loss of <10% for 30 wt% TPU samples), indicating that in the elastic regime, ABS matrix seems to dictate the overall mechanical properties of the material. Elongation at break follows an opposite trend, decreasing slightly for samples containing 10 wt% TPU and then increasing gradually for higher TPU contents. A plastic regime can be appreciated for samples containing 20 and 30 wt% TPU, allowing to reach higher elongations than for pure ABS. This implies that TPU is able to increase deformability of these materials. For 20 wt% TPU samples, lower elongations are obtained, but a yield strain value similar to pure ABS is obtained, while for 30 wt% TPU samples a significantly higher elongation can be obtained in exchange for a yield strain in the range of pure TPU. ANOVA analyses show that these three parameters are not significantly different for contents up to 20 wt% TPU when compared to pure ABS. Moreover, yield strength values are in agreement with the ones reported by the fabricant (29.3 MPa) and other authors (25–35 MPa) [13,33,50]. Thus, we assume that there is no loss in the mechanical properties of these blends behavior in a similar way than pure ABS. This also seems to indicate that for samples containing up to 20 wt% TPU, ABS governs the mechanical response, while for samples containing 30 wt % TPU, ABS only governs the elastic region. After the elongation at break of pure ABS ($5.8 \pm 0.3\%$) is surpassed, TPU governs the plastic region. Even though the presence of a plastic regime is clear, it is much shorter than for pure TPU, where extremely high elongations of almost 800% strain can be reached. As we showed in Fig. 3, we believe this is related with the loss in hydrogen bonds between TPU molecules, which is what provides the high deformability. This is also in well agreement with AFM phase results shown in Fig. 5g)–i), where we indicated the transition from an ABS matrix with well dispersed TPU for blends containing 10 wt% TPU to interconnected domains of TPU and ABS in the case of 30 wt% TPU blends. This looks a probable reason of why 30 wt % TPU can reach substantially higher elongation values, while 10 wt% TPU content makes the material even more brittle.

When we compare the mechanical properties for the XZ specimens, we see a completely different trend. Young's modulus does not decrease for samples containing 10 and 20 wt% TPU (differences are not significant according to ANOVA tests), while yield strength and elongation at break increase up to 2–3 times, when compared to pure ABS. Actually, stress-strain curves in Fig. 6b) for ABS:TPU blends show what it seem two different elastic regimes. At low strain values, the curves match quite well with pure ABS (except for blends containing 30 wt% TPU, where Young's modulus is slightly lower, Fig. 6c), but at strains above elongation at break of pure ABS ($1.0 \pm 0.2\%$) we observe a second elastic behavior, which enhances clearly the mechanical properties of the blends in this direction. Since it looks like a second elastic regime, with a lower Young's modulus, we hypothesize that this is caused by the presence of TPU, but also by its interactions with ABS matrix. We state that, as we showed in Fig. 3b), new supramolecular interactions appearing between ABS and TPU allow these blends to reach higher strength and elongation values, thus increasing the adhesive properties between layers. This is supported by the poor yield strength results for pure TPU, where we really had trouble to print self-standing specimens valid for tensile testing. We therefore conclude that what gives enhanced adhesive properties is the combination of ABS and TPU. ABS would act as a matrix, providing good mechanical properties, while TPU would create new interactions, besides providing more plasticity

to the material. This has a number of potential advantages, for instance in the fabrication of taller and more complex structures due to the better adhesion between layers.

SEM of the fracture surfaces of the different 1BA test specimens was performed. Fig. 7a) shows the fracture of pure ABS, where it can be appreciated a flat surface containing small pores characteristic of FFF printing corresponding to small gaps between fused filaments as a result of insufficient flow of the polymer melt during the deposition process. On the other hand, Fig. 7e) shows the fracture of pure TPU as a highly irregular surface. Contrary to pure ABS, shape of individual layers and roads can be barely identified, because of high plastic deformation of TPU before breaking. Fracture surface of XY specimens of blends containing ABS and TPU show an intermediate fracture behavior, as expected. As in the case of pure ABS, original shape of the deposited fused material can be identified, but a certain degree of plastic deformation can be observed, caused by the presence of TPU. This deformation seems to be homogeneous along the different layers. In general, in all cases it can be observed that the deposited filaments during the FFF process have been stretched until they have been broken and the fracture occurs within the layers. Fig. 7f)–j) shows fracture surfaces corresponding to the XZ specimens. In the case of ABS, it can be observed a quite flat surface (Fig. 7f)), and it can be identified some lines corresponding to the trajectory of the roads in one layer. Thus, the fracture in this case occurs because two contiguous layers are pulled apart. Fig. 7g)–i) shows that roughness of the surface raises when TPU content is increased. In particular, it can be observed layers at different heights in Fig. 7i), indicating that in this case, the fracture may be extended to more than one layer showing the potential ability of TPU to increase the adhesion between layers. We have already shown that compatibility of ABS and TPU is high and it enhances the mechanical properties (in particular, the tensile strength). This observed roughness seems to confirm a better interaction between layers, supporting the results observed in Fig. 6d). This effect is also observed for pure TPU in Fig. 7j). Thus, we can say that the yield strength measured for XZ specimens corresponds to the adhesion strength between two consecutive printed layers and therefore, interlayer adhesion is measured in these cases.

Finally, we evaluated the adhesive properties onto the platform by printing monolayers of 20 mm × 120 mm size. Platform temperature (T_b) was varied from room temperature (25 °C) to 90 °C and we obtained the minimum T_b needed for the proper printing of monolayers without using any fixation spray or other external help.

In Fig. 8 we observe that blends containing 10 wt% TPU need to be printed at least at 80 °C, practically the same minimum T_b than pure ABS. On the other hand, blends containing 30 wt% TPU allow successful printing at room temperature, i.e. in the same conditions as pure TPU. Blends containing 20 wt% TPU yield to an intermediate minimum T_b of 55 °C. Taking as a reference AFM phase results shown in Fig. 5g)–i), we can correlate these values to the phases observed, in a similar manner than we did to explain enhanced adhesion between layers by presence of TPU. We state that 10 wt% TPU blends do not possess enough TPU in surface and this TPU is quite well distributed within the ABS matrix having thus an overall behavior more like ABS. However, in 30 wt% TPU blends, TPU tends to aggregate in a higher degree, thus establishing more "sticky points" that allows the material to better adhere onto the platform. Blends containing 20 wt% TPU possess an intermediate, transition behavior that yields to an intermediate minimum T_b value for first layer adhesion. Moreover, we believe TPU can also interact via hydrogen bonding with the –OH polar groups present in the surface of the glass printing platform and form new supramolecular interactions in the same way than to ABS, as we showed with FTIR spectroscopy.

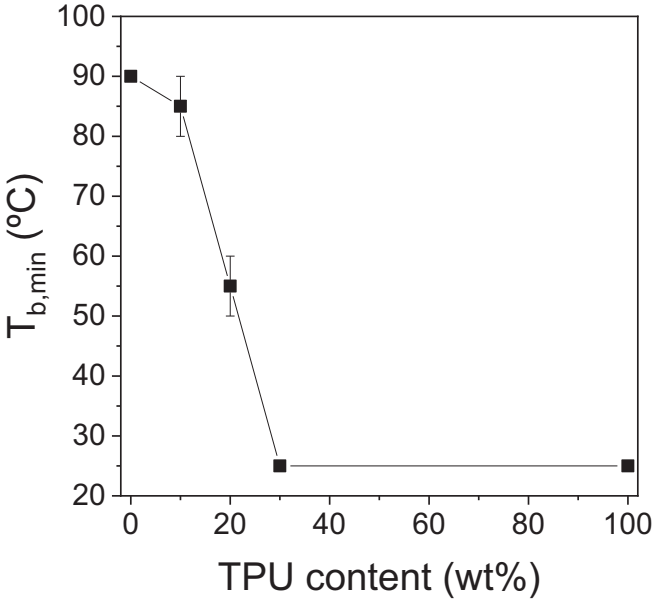

Fig. 8. Minimum platform temperature ($T_{b,min}$) required in FFF to ensure a correct adhesion of the first deposited layer as a function of TPU content.

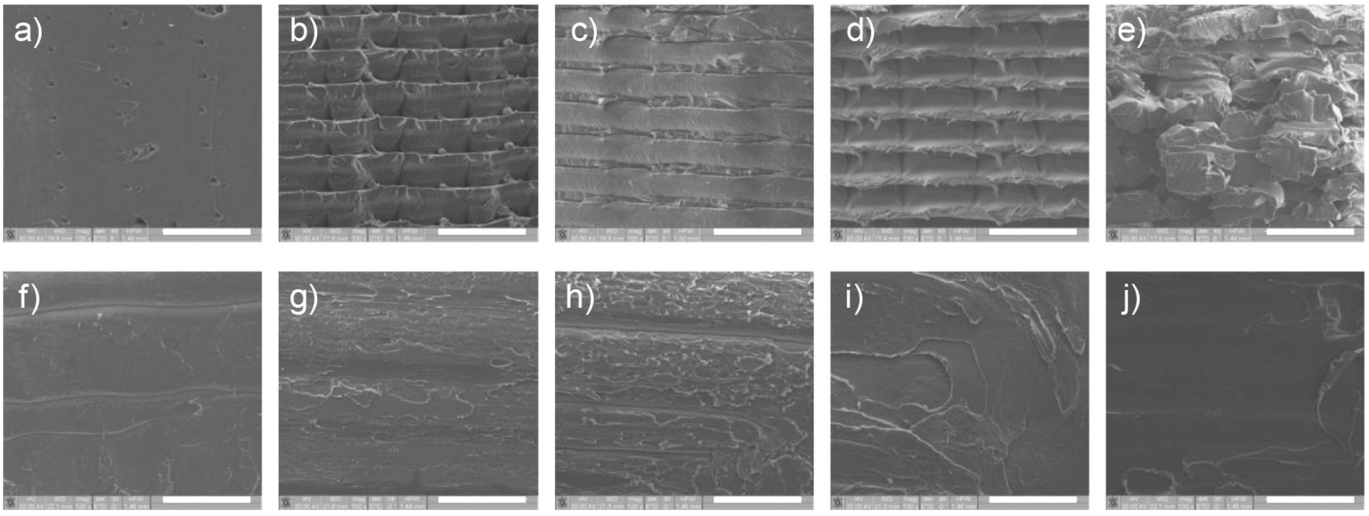

Fig. 7. SEM micrographs of fractures of 1BA test specimens printed in XY using a) pure ABS, ABS:TPU blends containing b) 10 wt% TPU, c) 20 wt% TPU, d) 30 wt% TPU and e) TPU; SEM micrographs of fractures of 1BA test specimens printed in XZ using f) pure ABS, ABS:TPU blends containing g) 10 wt% TPU, h) 20 wt% TPU, i) 30 wt% TPU and j) pure TPU. Scale bar: 500 μm.

However, printability at lower T_b values can vary mechanical properties due to faster cooling of the polymer melt. In order to evaluate this, monolayers containing 30 wt% TPU were printed at T_b values of 25 °C (room temperature) and 70 °C and their mechanical properties were tested. Fig. 9 shows that, regardless of the T_b used for printing, Young's modulus and yield strength are not statistically different and are in agreement with the results obtained in Fig. 6. However, elongation at break not only decreases but is enhanced from 21.4 ± 7.9 to 47.5 ± 13.9% strain. Therefore, decreasing T_b presents a number of advantages when printing ABS:TPU blends: first, it speeds up the printing process eliminating the waiting time up to high temperature values; second, it eliminates (or diminishes when blends for TPU content below 30 wt% is used) the energetic cost of increasing T_b; third, it not only decreases but it enhances some of the mechanical properties obtained.

4. Conclusions

In this work we have prepared different blends suitable for FFF containing ABS and TPU. We have studied the compositional distribution of the objects printed by FTIR, Raman microscopy and AFM. We demonstrated that these blends present a homogeneous distribution of ABS and TPU, probably caused by hydrogen bonding supramolecular interactions between TPU polar groups and ABS acrylonitrile and aromatic moieties. AFM phase images showed that when TPU content is 10 wt%, it is homogeneously distributed within the ABS matrix, while for blends containing 30 wt% TPU, it tends to form a continuous phase along the ABS matrix. We have correlated this compositional study with the mechanical properties observed in tensile testing specimens printed by FFF. We state that presence of TPU increases interlayer adhesion (bonding strength) between printed layers while it does not decrease the yield strength value for contents up to 20 wt%. For blends containing 30 wt% TPU this adhesion is also enhanced, but yield strength is more similar to pure TPU than ABS. However, this high content of TPU leads to enhanced adhesion onto the printing platform allowing to keep it at room temperature. Thus, we conclude these blends are promising candidates as materials with enhanced adhesion (between layers and to the platform) to be used in FFF. Due to their commercial availability and simple preparation of the blends, we believe these materials are particular interesting for large-scale, industrial applications as an alternative to pure ABS.

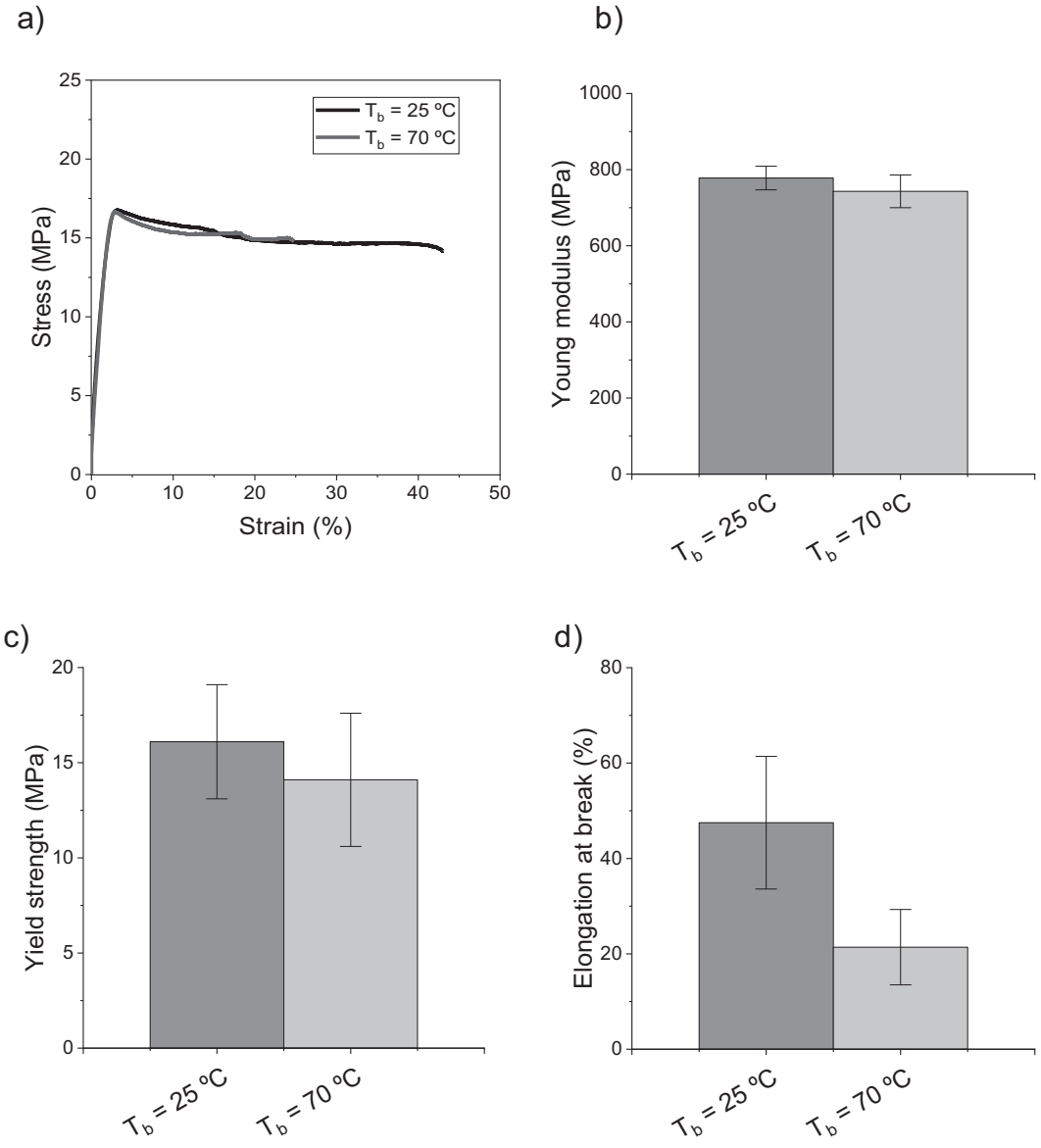

Fig. 9. a) Representative strain-stress curves, b) Young's modulus, c) yield strength and d) elongation at break of monolayers of ABS:TPU blends containing 30 wt% TPU at 70 °C and 25 °C.

Acknowledgements

This work was funded by Ministry of Science, Innovation and Universities (project TEC2017-86102-C2-2-R) and Junta de Andalucía (Research group INNANOMAT, ref. TEP-946). Co-funding from EU is also acknowledged. A.S. de León also acknowledges the same Ministry for his Juan de la Cierva postdoctoral fellowship (FJCI-2016-29330). Authors would like to thank H. Bakkali and M. Domínguez for AFM measurements.

References

[1] S.C. Ligon, R. Liska, J. Stampfl, M. Gurr, R. Mülhaupt, Polymers for 3D printing and customized additive manufacturing, Chem. Rev. 117 (2017) 10212–10290, https://doi.org/10.1021/acs.chemrev.7b00074.
[2] S.A.M. Tofail, E.P. Koumoulos, A. Bandyopadhyay, S. Bose, L. O'Donoghue, C. Charitidis, Additive manufacturing: scientific and technological challenges, market uptake and opportunities, Mater. Today 21 (2018) 22–37, https://doi.org/10.1016/j.mattod.2017.07.001.
[3] P. Rastogi, B. Kandasubramanian, Breakthrough in the printing tactics for stimuli-responsive materials: 4D printing, Chem. Eng. J. 366 (2019) 264–304, https://doi.org/10.1016/j.cej.2019.02.085.
[4] I. Durgun, R. Ertan, Experimental investigation of FDM process for improvement of mechanical properties and production cost, Rapid Prototyp. J. 20 (2014) 228–235, https://doi.org/10.1108/RPJ-10-2012-0091.
[5] B. Ben Difallah, M. Kharrat, M. Dammak, G. Monteil, Mechanical and tribological response of ABS polymer matrix filled with graphite powder, Mater. Des. 34 (2012) 782–787, https://doi.org/10.1016/j.matdes.2011.07.001.
[6] M. Nikzad, S.H. Masood, I. Sbarski, Thermo-mechanical properties of a highly filled polymeric composites for fused deposition modeling, Mater. Des. 32 (2011) 3448–3456, https://doi.org/10.1016/j.matdes.2011.01.056.
[7] K. Akato, C.D. Tran, J. Chen, A.K. Naskar, Poly (ethylene oxide)-assisted macromolecular self-assembly of lignin in ABS matrix for sustainable composite applications, ACS Sustain. Chem. Eng. 3 (2015) 3070–3076, https://doi.org/10.1021/acssuschemeng.5b00509.
[8] H.L. Tekinalp, V. Kunc, G.M. Velez-Garcia, C.E. Duty, L.J. Love, A.K. Naskar, C.A. Blue, S. Ozcan, Highly oriented carbon fiber-polymer composites via additive manufacturing, Compos. Sci. Technol. 105 (2014) 144–150, https://doi.org/10.1016/j.compscitech.2014.10.009.
[9] O.A. Mohamed, S.H. Masood, J.L. Bhowmik, Experimental investigation of time-dependent mechanical properties of PC-ABS prototypes processed by FDM additive manufacturing process, Mater. Lett. 193 (2017) 58–62, https://doi.org/10.1016/j.matlet.2017.01.104.
[10] M. Dawoud, I. Taha, S.J. Ebeid, Mechanical behaviour of ABS: an experimental study using FDM and injection moulding techniques, J. Manuf. Process. 21 (2016) 39–45, https://doi.org/10.1016/j.jmapro.2015.11.002.
[11] M.F. Arif, S. Kumar, K.M. Varadarajan, W.J. Cantwell, Performance of biocompatible PEEK processed by fused deposition additive manufacturing, Mater. Des. 146 (2018) 249–259, https://doi.org/10.1016/j.matdes.2018.03.015.
[12] Y. Song, Y. Li, W. Song, K. Yee, K.-Y. Lee, V.L. Tagarielli, Measurements of the mechanical response of unidirectional 3D-printed PLA, Mater. Des. 123 (2017) 154–164, https://doi.org/10.1016/j.matdes.2017.03.051.
[13] Z. Weng, J. Wang, T. Senthil, L. Wu, Mechanical and thermal properties of ABS/montmorillonite nanocomposites for fused deposition modeling 3D printing, Mater. Des. 102 (2016) 276–283, https://doi.org/10.1016/j.matdes.2016.04.045.
[14] S.-H. Ahn, M. Montero, D. Odell, S. Roundy, P.K. Wright, Anisotropic material properties of fused deposition modeling ABS, Rapid Prototyp. J. 8 (2002) 248–257, https://doi.org/10.1108/13552540210441166.
[15] E. Provaggi, C. Capelli, B. Rahmani, G. Burriesci, D.M. Kalaskar, 3D printing assisted finite element analysis for optimising the manufacturing parameters of a lumbar fusion cage, Mater. Des. 163 (2019), 107540. https://doi.org/10.1016/j.matdes.2018.107540.
[16] V. Damodaran, A.G. Castellanos, M. Milostan, P. Prabhakar, Improving the mode-II interlaminar fracture toughness of polymeric matrix composites through additive manufacturing, Mater. Des. 157 (2018) 60–73, https://doi.org/10.1016/j.matdes.2018.07.006.
[17] T.D. McLouth, J.V. Severino, P.M. Adams, D.N. Patel, R.J. Zaldivar, The impact of print orientation and raster pattern on fracture toughness in additively manufactured ABS, Addit. Manuf. 18 (2017) 103–109, https://doi.org/10.1016/j.addma.2017.09.003.
[18] A. Le Duigou, M. Castro, R. Bevan, N. Martin, 3D printing of wood fibre biocomposites: from mechanical to actuation functionality, Mater. Des. 96 (2016) 106–114, https://doi.org/10.1016/j.matdes.2016.02.018.
[19] C. Koch, L. Van Hulle, N. Rudolph, Investigation of mechanical anisotropy of the fused filament fabrication process via customized tool path generation, Addit. Manuf. 16 (2017) 138–145, https://doi.org/10.1016/j.addma.2017.06.003.
[20] D.-A. Türk, F. Brenni, M. Zogg, M. Meboldt, Mechanical characterization of 3D printed polymers for fiber reinforced polymers processing, Mater. Des. 118 (2017) 256–265, https://doi.org/10.1016/j.matdes.2017.01.050.
[21] N.P. Levenhagen, M.D. Dadmun, Bimodal molecular weight samples improve the isotropy of 3D printed polymeric samples, Polymer (Guildf) 122 (2017) 232–241, https://doi.org/10.1016/j.polymer.2017.06.057.
[22] N.P. Levenhagen, M.D. Dadmun, Interlayer diffusion of surface segregating additives to improve the isotropy of fused deposition modeling products, Polymer (Guildf) 152 (2018) 35–41, https://doi.org/10.1016/j.polymer.2018.01.031.
[23] N. Aliheidari, R. Tripuraneni, A. Ameli, S. Nadimpalli, Fracture resistance measurement of fused deposition modeling 3D printed polymers, Polym. Test. 60 (2017) 94–101, https://doi.org/10.1016/j.polymertesting.2017.03.016.
[24] J. Zhu, Y. Hu, Y. Tang, B. Wang, Effects of styrene–acrylonitrile contents on the properties of ABS/SAN blends for fused deposition modeling, J. Appl. Polym. Sci. 134 (2017)https://doi.org/10.1002/app.44477.
[25] C.S. Davis, K.E. Hillgartner, S.H. Han, J.E. Seppala, Mechanical strength of welding zones produced by polymer extrusion additive manufacturing, Addit. Manuf. 16 (2017) 162–166, https://doi.org/10.1016/j.addma.2017.06.006.
[26] J.C. Riddick, M.A. Haile, R. Von Wahlde, D.P. Cole, O. Bamiduro, T.E. Johnson, Fractographic analysis of tensile failure of acrylonitrile-butadiene-styrene fabricated by fused deposition modeling, Addit. Manuf. 11 (2016) 49–59, https://doi.org/10.1016/j.addma.2016.03.007.
[27] C. Shemelya, A. De La Rosa, A.R. Torrado, K. Yu, J. Domanowski, P.J. Bonacuse, R.E. Martin, M. Juhasz, F. Hurwitz, R.B. Wicker, B. Conner, E. Mac Donald, D.A. Roberson, Anisotropy of thermal conductivity in 3D printed polymer matrix composites for space based cube satellites, Addit. Manuf. 16 (2017) 186–196, https://doi.org/10.1016/j.addma.2017.05.012.
[28] A. Kantaros, D. Karalekas, Fiber Bragg grating based investigation of residual strains in ABS parts fabricated by fused deposition modeling process, Mater. Des. 50 (2013) 44–50, https://doi.org/10.1016/j.matdes.2013.02.067.
[29] M.A. Nazan, F.R. Ramli, M.R. Alkahari, M.A. Abdullah, M.N. Sudin, An exploration of polymer adhesion on 3D printer bed, IOP Conf. Ser. Mater. Sci. Eng. 210 (2017), 012062. https://doi.org/10.1088/1757-899X/210/1/012062.
[30] M.G. Tadesse, D. Dumitrescu, C. Loghin, Y. Chen, L. Wang, V. Nierstrasz, 3D printing of ninja flex filament onto PEDOT: PSS-coated textile fabrics for electroluminescence applications, J. Electron. Mater. 47 (2018) 2082–2092, https://doi.org/10.1007/s11664-017-6015-6.
[31] C.R. Rocha, A.R. Torrado Perez, D.A. Roberson, C.M. Shemelya, E. Macdonald, R.B. Wicker, Novel ABS-based binary and ternary polymer blends for material extrusion 3D printing, J. Mater. Res. 29 (2014) 1859–1866, https://doi.org/10.1557/jmr.2014.158.
[32] J. Yin, C. Lu, J. Fu, Y. Huang, Y. Zheng, Interfacial bonding during multi-material fused deposition modeling (FDM) process due to inter-molecular diffusion, Mater. Des. 150 (2018) 104–112, https://doi.org/10.1016/j.matdes.2018.04.029.
[33] A.C. Abbott, G.P. Tandon, R.L. Bradford, H. Koerner, J.W. Baur, Process-structure-property effects on ABS bond strength in fused filament fabrication, Addit. Manuf. 19 (2018) 23–38, https://doi.org/10.1016/j.addma.2017.11.002.
[34] R. Gautam, S. Idapalapati, S. Feih, Printing and characterisation of Kagome lattice structures by fused deposition modelling, Mater. Des. 137 (2018) 266–275, https://doi.org/10.1016/j.matdes.2017.10.022.
[35] F.C. Wang, M. Feve, T.M. Lam, J.-P. Pascault, FTIR analysis of hydrogen bonding in amorphous linear aromatic polyurethanes. I. Influence of temperature, J. Polym. Sci. Part B Polym. Phys. 32 (1994) 1305–1313, https://doi.org/10.1002/polb.1994.090320801.
[36] Y. Xu, Z. Petrovic, S. Das, G.L. Wilkes, Morphology and properties of thermoplastic polyurethanes with dangling chains in ricinoleate-based soft segments, Polymer (Guildf) 49 (2008) 4248–4258, https://doi.org/10.1016/j.polymer.2008.07.027.
[37] M.A. Hood, B. Wang, J.M. Sands, J.J. La Scala, F.L. Beyer, C.Y. Li, Morphology control of segmented polyurethanes by crystallization of hard and soft segments, Polymer (Guildf) 51 (2010) 2191–2198, https://doi.org/10.1016/j.polymer.2010.03.027.
[38] D. Xu, H. Lu, Q. Huang, B. Deng, L. Li, Flame-retardant effect and mechanism of melamine phosphate on silicone thermoplastic elastomer, RSC Adv. 8 (2018) 5034–5041, https://doi.org/10.1039/c7ra12865g.
[39] Q. Chen, J.D. Mangadlao, J. Wallat, A. De Leon, J.K. Pokorski, R.C. Advincula, 3D printing biocompatible polyurethane/poly (lactic acid)/graphene oxide nanocomposites: anisotropic properties, ACS Appl. Mater. Interfaces 9 (2017) 4015–4023, https://doi.org/10.1021/acsami.6b11793.
[40] M. Saggu, N.M. Levinson, S.G. Boxer, Experimental quantification of electrostatics in X-H···φ hydrogen bonds, J. Am. Chem. Soc. 134 (2012) 18986–18997, https://doi.org/10.1021/ja305575t.
[41] S. Parnell, K. Min, M. Cakmak, Kinetic studies of polyurethane polymerization with Raman spectroscopy, Polymer (Guildf) 44 (2003) 5137–5144, https://doi.org/10.1016/S0032-3861(03)00468-3.
[42] J. Jyoti, S. Basu, B.P. Singh, S.R. Dhakate, Superior mechanical and electrical properties of multiwall carbon nanotube reinforced acrylonitrile butadiene styrene high performance composites, Compos. Part B Eng. 83 (2015) 58–65, https://doi.org/10.1016/j.compositesb.2015.08.055.
[43] A.S. De León, A. Del Campo, M. Fernández-García, J. Rodríguez-Hernández, A. Muñoz-Bonilla, Fabrication of structured porous films by breath figures and phase separation processes: tuning the chemistry and morphology inside the pores using click chemistry, ACS Appl. Mater. Interfaces 5 (2013) 3943–3951, https://doi.org/10.1021/am400679r.
[44] A. Taguet, M.A. Huneault, B.D. Favis, Interface/morphology relationships in polymer blends with thermoplastic starch, Polymer (Guildf) 50 (2009) 5733–5743, https://doi.org/10.1016/j.polymer.2009.09.055.
[45] B. Ohlsson, H. Hassander, B. Törnell, Improved compatibility between polyamide and polypropylene by the use of maleic anhydride grafted SEBS, Polymer (Guildf) 39 (1998) 6705–6714, https://doi.org/10.1016/S0032-3861(97)10290-7.
[46] J.H. Park, S.C. Jana, The relationship between nano- and micro-structures and mechanical properties in PMMA-epoxy-nanoclay composites, Polymer (Guildf) 44 (2003) 2091–2100, https://doi.org/10.1016/S0032-3861(03)00075-2.

[47] A. Muñoz-Bonilla, E. Ibarboure, E. Papon, J. Rodriguez-Hernandez, Self-organized hierarchical structures in polymer surfaces: self-assembled nanostructures within breath figures, Langmuir 25 (2009) 6493–6499, https://doi.org/10.1021/la9003214.
[48] S.-L. Gao, E. Mäder, Characterisation of interphase nanoscale property variations in glass fibre reinforced polypropylene and epoxy resin composites, Compos. A: Appl. Sci. Manuf. 33 (2002) 559–576, https://doi.org/10.1016/S1359-835X(01)00134-8.
[49] G.K. Bar, G.F. Meyers, The application of atomic force microscopy to the characterization of industrial polymer materials, MRS Bull. 29 (2004) 464–470, https://doi.org/10.1557/mrs2004.140.
[50] J.R.C. Dizon, A.H. Espera, Q. Chen, R.C. Advincula, Mechanical characterization of 3D-printed polymers, Addit. Manuf. 20 (2018) 44–67, https://doi.org/10.1016/j.addma.2017.12.002.